Processing and Application of Ceramics 11 [2] (2017) 136–146
https://doi.org/10.2298/PAC1702136R



# *In vitro* bioactivity of glass-ceramic/fibroin composites

Lachezar Radev[1,*], Irena Michailova[2], Silviya Stateva[3], Diana Zaimova[1], Hristo Georgiev[4], Margarita Apostolova[3]

[1]*Department of Fundamental Chemical Technology, University of Chemical Technology and Metallurgy, Sofia, Bulgaria*
[2]*Department of Silicate Technology, University of Chemical Technology and Metallurgy, Sofia, Bulgaria*
[3]*Roumen Tsanev Institute of Molecular Biology, Bulgarian Academy of Sciences, Sofia, Bulgaria*
[4]*Department of Polymer Engineering, University of Chemical Technology and Metallurgy, Sofia, Bulgaria*

Received 24 October 2016; Received in revised form 25 March 2017; Accepted 17 May 2017

## Abstract

*Bioactive composite materials were prepared by mixing 20 wt.% of silk fibroin (SF) and 80 wt.% of glass-ceramics from $CaO$-$SiO_2$-$P_2O_5$-$MgO$ system. In vitro bioactivity of the prepared composites was evaluated in 1.5 simulated body fluid (1.5 SBF) in static conditions. The obtained samples before and after in vitro tests were characterized by X-ray diffraction (XRD) analysis, Fourier transform infrared spectroscopy (FTIR), and X-ray photoelectron spectroscopy (XPS). The changes in 1.5 SBF solutions after soaking the samples were evaluated by inductively coupled plasma atomic emission spectroscopy (ICP-AES). MG63 osteosarcoma cells were used for the biological experiments. The obtained experimental data proved that the synthesized composites exhibit excellent in vitro bioactivity.*

***Keywords:*** *biomaterials, fibroin, glass-ceramics, in vitro bioactivity*

## I. Introduction

It is well known that natural bone is a typical inorganic/organic composite containing approximately 80% hydroxyapatite (HA) and 20% collagen matrix [1]. In this context, HA has attracted much attention for large bone defects regeneration [2,3] due to its excellent osteoconductivity and similarity to the mineral phase of bone. Nevertheless, its low compressive strength limits its application to non low-load bearing bone repairs [4].

In recent years, much attention has been paid to the fabrication of functional scaffolds from natural polymers, such as collagen [5], gelatin [6], alginate [7], polylactic acid [8], polyamide [9], and silk fibroin (SF) [10–16], which can be incorporated together with HA to achieve both porosity and mechanical strength.

Among them SF is of a practical interest due to its excellent intrinsic properties utilizable in the biotechnological and biomedical fields. On the other hand, it is known that SF is composed of 17 aminoacids. It has been proved that SF is a good biocompatible material, which has been successfully used for various medical applications. Kong *et at.* [11] demonstrated that silk fibres could induce HA nucleation on the surfaces proteins in simulated body fluid (SBF) solution at pH = 8. The authors also proved that there are strong chemical bonds between SF and HA. For this reason, a co-precipitation method was often used to synthesize silk powder/HA nanocomposites [11,17–23]. For instance, Wang *et al.* [18] deposited HA on fibroin microspheres through the co-precipitation method. Furuzono *et al.* [24] developed a HA/F composite, where fibroin was modified with organic compound. In another article Kino *et al.* [25] reported that the regenerated fibroin films containing $Ca^{2+}$ ions were coated with HA, after soaking in 1.5 SBF for 6 h. Li *et al.* [26] proved that fibroin can induce HA deposition at 37 °C in 1.5 SBF. The effect of pH and initial $Ca^{2+}$–$H_2PO_4^-$ concentration on the crystal growth of HA in the presence of SF is studied by Ren *et al.* [21]. They evaluate the effect of pH and initial $Ca^{2+}$ and $PO_4^{3-}$ concentration on the products of SF mineralization. They also demonstrated that pH = 7 promote the transition of dicalcium phosphate dihydrate (DCPD) to HA. On the other hand, Kong *et al.* [27] observed that SF can accelerate the phase trans-

*Corresponding author: tel: +35 92 816 3280,
fax: +35 92 868 5488, e-mail: *l_radev@abv.bg*

mittance of amorphous calcium phosphate (ACP) to the crystal hybrid between DCPD and HA. Li *et al.* [28] synthesized SF/calcium phosphate composite by adding the different amount of $Na_2SiO_3$ to investigate the effect of silicon on the HA formation in the composite. Based on the obtained results they concluded that the addition of silicon could accelerate the HA formation. SF/wollastonite scaffolds were prepared by Zhu *et al.* [29] via freeze-drying method. They showed that the composite scaffold was *in vitro* bioactive, because wollastonite induced the formation of carbonate containing hydroxyapatite ($CO_3$HA) on the surface of the samples, after soaking in SBF solution for 5 days [29]. Four types of hybrid films were fabricated by Vachiraroj *et al.* [30]. These materials include gelatine conjugated SF, HA/SF, HA/gelatin/SF, and HA/chitosan. The prepared films were investigated in terms of *in vitro* adhesion, proliferation and osteogenic differentiation with preosteoblast cell lines (MC3T3-E1) and rat bone marrow derived stem cells (MC3). The authors proved that MC3T3-E1 showed higher proliferation rate [30].

In our previous work [31], we have prepared some *in vitro* bioactive composites between glass-ceramics from CaO-$SiO_2$-$P_2O_5$ system and SF solution and evaluated apatite formation on their surface, after soaking in SBF solution. The purpose of the present article is to prepare novel glass-ceramics/SF bioactive composites, based on two types of glass-ceramics (from CaO-$SiO_2$-$P_2O_5$-MgO system, analysed in our previous paper [32]), and to evaluate their *in vitro* bioactivity in 1.5 SBF solution after 14 days of soaking in static conditions. The novelty of the presented work is that the glass-ceramics were previously soaked in TRIS-HCl solution for 14 days, and in this form used for preparation of the bioactive composites. In this context, we try to discuss the main question - how the phase composition of the synthesized samples influences the structure and *in vitro* bioactivity?

## II. Experimental Part

### *2.1. Preparation of glass-ceramics/SF composites*

Bioactive glass-ceramic/SF composites were prepared by mixing 20 wt.% of silk fibroin (SF) and 80 wt.% of glass-ceramics from CaO-$SiO_2$-$P_2O_5$-MgO system. Silk fibroin (SF) solution was prepared by dissolving fibroin without sericin in 9 M LiBr at 60 °C for 4 h and then dialysed against distilled water at room temperature for 3 days using cellulose membrane (MWCO 12000 Da) for 72 h to remove the salts [30]. The final concentration of the SF solution was 3 wt.%, in accordance with literature data [29].

After that two glass-ceramic powders from CaO-$SiO_2$-$P_2O_5$-MgO system (denoted as C1 and C2), as inorganic part of the composites, were synthesized via multi step sol-gel method. The powders have different compositions, i.e. C1 contains 38 wt.% CaO, 29 wt.% $SiO_2$, 31 wt.% $P_2O_5$ and 2 wt.% MgO, whereas C2 contains 55 wt.% CaO, 20 wt.% $SiO_2$, 22 wt.% $P_2O_5$ and 3 wt.% MgO. In the first step $SiO_2$ sol was obtained from tetraethoxysilane (TEOS) by mixing with solvent (mixture of $C_2H_5OH$ and $H_2O$) and a catalyst (a small amount of HCl) in a volume ratio TEOS : $C_2H_5OH$ : $H_2O$ : HCl = 1 : 1 : 1 : 0.01. After approximately 1 h and the formation of transparent solution, the magnesium salt ($Mg(NO_3)_2 \times 6\,H_2O$) was dissolved in water and added to the prehydrolysed TEOS under stirring for 14 h. In the second step calcium phosphate (CP) solution was prepared by mixing $Ca(OH)_2$ and $H_3PO_4$ at pH = 10–11. The calcium phosphate mixture was added dropwise into the modified silica sol under intensive stirring. The prepared mixed sol was stirred for 24 h, gelled at 120 °C for 12 h and thermally treated at 1200 °C for 2 h in a tubular furnace. The structure evolution of the thermally treated samples was presented in our previous paper [32]. The obtained glass-ceramics was soaked in TRIS-HCl buffer for 14 days [32].

Organic/inorganic composites were prepared by mixing of the treated glass-ceramics and SF solution without binding agents. A certain amount of C1 or C2 glass-ceramic powder was added into the SF solution (using weight ratio C : SF = 80 : 20) under stirring for 4 h in order to disperse the glass-ceramic particles uniformly. The obtained mixture was poured into plastic cup. The mixture was frozen at −60 °C and then lyophilized. Finally, two samples were obtained and denoted as C1F and C2F.

### *2.2. In vitro bioactivity of the prepared composites*

*In vitro* bioactivity of C1F and C2F samples was evaluated by examining the apatite formation on their surfaces in 1.5 SBF solutions. 1.5 SBF solution was prepared by using the following reagents: NaCl = 11.9925 g, $NaHCO_3$ = 0.5295 g, KCl = 0.3360 g, $K_2HPO_4 \times 3\,H_2O$ = 0.3420 g, $MgCl_2 \times 6\,H_2O$ = 0.4575 g, $CaCl_2 \times 2\,H_2O$ = 0.5520 g, $Na_2SO_4$ = 0.1065 g and buffering at pH = 7.25 at 36.5 °C with TRIS = 9.0075 g and 1 M HCl in distilled water. The synthesized composites were immersed in 1.5 SBF solution at human body temperature (36.6 °C) in polyethylene bottles in static conditions for 14 days. After soaking they were removed from the fluid, gently rinsed with distilled water, and dried at 37 °C for 12 h.

The structure and *in vitro* bioactivity of the synthesized C1F and C2F composites were studied by FTIR, XRD, ICP-AES and XPS. Powder X-ray diffraction spectra were collected within the $2\theta$ range from 10° to 80° with a constant step of 0.04° and counting time of 1 s/step on a Bruker D8 Advance diffractometer with Cu$K\alpha$ radiation and SolX detector. The spectra were evaluated with the Diffrac*plus* EVA package. FTIR transmission spectra were recorded by using a Brucker Tensor 27 spectrometer with scanner velocity 10 kHz. Diluted pellets of KBr were prepared by mixing of ~1 mg of the samples with 300 mg KBr. Transmission spectra were recorded using MCT detector with

64 scans and 1 $cm^{-1}$ resolution. The ionic concentrations of Ca, P, Si, and Mg of these solutions were determined by inductively coupled plasma atomic emission spectroscopy (ICP-AES), Iris 1000, Thermo Elemental, USA. X-ray photoelectron spectroscopy (XPS) of the samples after *in vitro* test in 1.5 SBF solution for 14 days was carried out using ESCALAB MkII (VG Scientific) electron spectrometer at a base pressure in the analysis chamber of $5\times10^{-10}$ mbar (during the measurement $1\times10^{-8}$ mbar), using AlK X-ray source (excitation energy $h\nu$ = 1486.6 eV). The pass energy of the hemispherical analyser was 20 eV, 6 mm slit widths (entrance/exit). The instrumental resolution measured as the full width at half maximum of the Ag3d5/2, photoelectron peak is 1 eV [33]. The energy scale is corrected to the C1s - peak maximum at 285.0 eV for electrostatic charging. The processing of the measured spectra includes a subtraction of X-ray satellites and Shirley-type background [34]. The peak positions and areas are evaluated by a symmetrical Gaussian-Lorentzian curve fitting. The relative concentrations of the different chemical species are determined based on normalization of the peak areas to their photoionization cross-sections, calculated by Scofield [34].

### 2.3. Cell culture and treatment

Human osteosarcoma cells MG63 cells (MG63, CRL-1427) were used for these experiments. MG63 have been well characterized, and widely used for testing biomaterials. In order to limit the differences in phenotypic expression, the cells were used at a passage 10 to 15. The cells were maintained in Eagle's Minimum Essential Medium (MEM, Lonza, Switzerland) containing 10% heat-inactivated fetal bovine serum (FBS, Lonza, Switzerland), 100 units/ml penicillin, and 100 μg/ml streptomycin in a humidified $CO_2$ atmosphere at 37 °C. They were routinely checked for mycoplasma contamination by 4′,6-Diamidin-2-phenylindol staining (DAPI, Roche Diagnostics, Mannheim, Germany) and were found free of it. The microscopy was performed with a Carl Zeiss AM240 microscope equipped with Zeiss AxioCamM-Rmand Andor (iXon+) cameras.

In all experiments the initial cell number was $1\times10^5$ cells/ml. C1F and C2F samples were added in concentrations up to 10 μg/$cm^2$. It was not possible to guarantee that the particles were evenly distributed in the well plates, the experiments were conducted in triplicate to minimize any gross errors caused by uneven distribution of the particles.

The cell growth and the cytotoxicity of C1F and C2F composites were determined by MTT assays [35]. 300 μl MTT solution (5 mg/ml) was added to each sample, where MG63 cells were growing for up to 72 h treated with different C1F and C2F concentrations. They were further incubated for 3 h at 37 °C in order to dissolve the formazan product of the MTT reduction by the cellular enzymes, the cell media was removed and 300 μl/well of 100% anhydrous isopropanol was added. Following the complete extraction of formazan the optical density of the obtained solutions was measured at 550/630 nm with a DTX880 spectrophotometer (Beckman Coulter, USA). The results were used to calculate the cell growth by the OriginLab program.

### 2.4. Detection and quantification of mineralization

The detection and quantification of the mineralization were performed as described by Gregory *et al.* [36] with some modifications. Monolayers of MG63 were plated in 48-well plates in osteoprogenitor media (Lonza) up to 21 days. Following different periods of treatment with 10 μg/$cm^2$ of C1F or C2F, the cells were washed with phosphate-buffered solution (PBS) and fixed in 10% (v/v) formaldehyde (Sigma-Aldrich) for 15 min on ice. The monolayers were washed twice with $dH_2O$ prior to addition of 0.5 ml of 40 mM Alizarin Red S (ARS) (pH 4.1 adjusted with ammonium hydroxide) per well. The plates were further incubated for 20 minutes at room temperature with gentle shaking. After complete aspiration of the unincorporated dye, the wells were washed five times with $dH_2O$. Stained monolayers were visualized by phase microscopy.

Intracellular ALP activity was analysed by a commercial colorimetric ALP activity detection kit (Abcam, ab83369) following the manufacturer's instructions. ALP activity was further normalized by mg intracellular protein content.

The data were evaluated by analysis of variance (ANOVA) followed by Bonferroni's post-hock test. Differences in the results at the level of $p < 0.05$ were considered statistically significant. The statistical analysis was carried out using the PASW 18.0 statistical software package (IBM) for Windows.

## III. Results and discussion

### 3.1. Samples before in vitro test in 1.5 SBF solution

XRD patterns of C1F and C2F samples are presented in Figs. 1 and 2. In the C1F sample XRD proved the presence of whitlockite ($(Ca,Mg)_3(PO_4)_2$), PDF card 70-2064, cristobalite ($SiO_2$), PDF card 85-0512, and silicocarnotite ($Ca_5(PO_4)_2SiO_4$), PDF card 40-0293. Furthermore, in the C2F sample, XRD confirmed the presence of HA ($Ca_{10}(PO_4)_6(CO_3)\times\frac{1}{2}(OH)$), PDF card 01-072-7532 and hydromagnezite ($Mg_5(CO_3)_4(OH)_2\times4\,H_2O$), PDF card 25-0513.

Based on our preliminary results on the two glass-ceramics from $CaO\text{-}SiO_2\text{-}P_2O_5\text{-}MgO$ system, we can conclude that HA and hydromagnezite were formed on the surface of the soaked samples in TRIS-HCl buffer [32]. If we compare XRD results for the C1 and C2 glass-ceramics, soaked in TRIS-HCl buffer, published in [32], with these in the present study (Figs. 1 and 2), it will be seen that HA in the C1F and C2F composites has low crystallinity. This fact could be related with the process of partial dissolution of HA under experimental

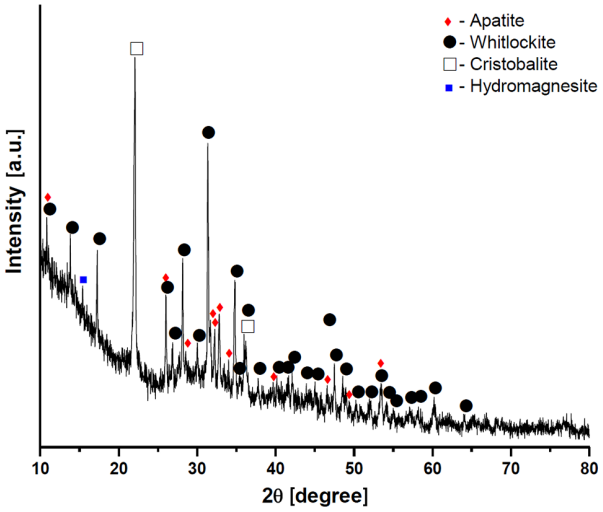


**Figure 1. XRD pattern of C1F sample, before *in vitro* test**

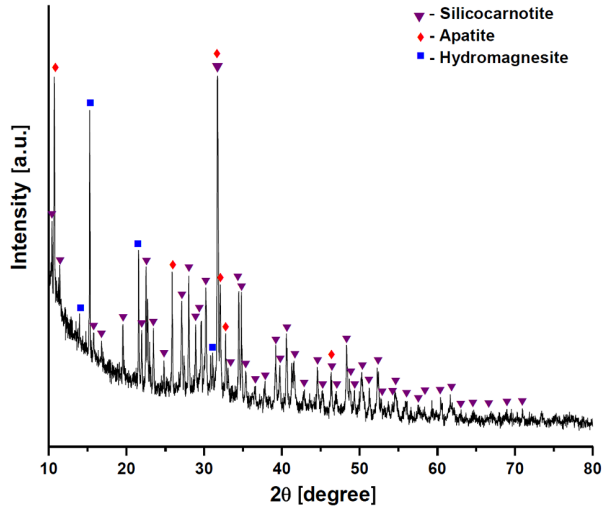


**Figure 2. XRD pattern of C2F sample, before *in vitro* test**

conditions [37,38].

Structural changes for both parts (SF and glass-ceramics) of the synthesized composites were investigated by FTIR (Fig. 3). First of all, the FTIR spectra of the obtained composites, presented in Fig. 3, show very complicated character. Silk fibroin (SF), as the organic part of the two composites, displayed strong adsorption peaks, posited at 1620 $cm^{-1}$ and 1538 $cm^{-1}$ (for the C1F sample) and 1622 $cm^{-1}$ and 1541 $cm^{-1}$ (for the C2F sample). The observed peaks are characteristic for $\beta$-sheet conformation of fibroin [15,39]. The peak at 1286 $cm^{-1}$ (for the C2F sample) is a characteristic peak of amide III [14]. Surprisingly, the bands for amide III disappeared in the C1F sample, as it can be seen from Fig. 3 (curve a). Xe and *et al.* [14] also observed that the bands, which are related to amide II and amide III, disappeared in the synthesized SF/HA composites. There is another explanation for the disappearance of amide III in our C1F sample. It is based on the research of chitosan/SF blends, studied by Ramya *et al.* [40]. The authors have synthesized chitosan/SF blends by the mixing of chitosan and SF in a ratio 1 : 1 and they concluded that the disappearance of the band at 1628 $cm^{-1}$ (amide I) could be related to the formation of intramolecular bond between chitosan and SF [40]. In our case, the disappearance of amide III for the C1F sample could be explained by the formation of strong hydrogen bonds between OH groups of the Ca-deficient HA which is formed on the C1 glass-ceramic surface after soaking in TRIS-HCl buffer for 14 days in static conditions [32].

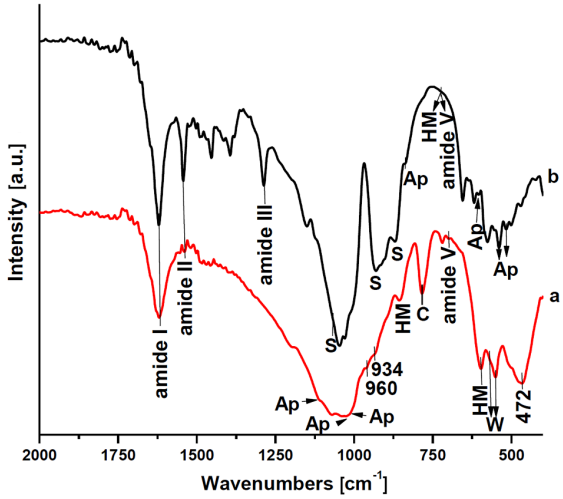


**Figure 3. FTIR spectra of C1F (a) and C2F (b) composites before *in vitro* test**

On the other hand, in the FTIR spectrum of the C1F composite (Fig. 3, curve a), the slightly visible peak at 782 $cm^{-1}$ and those at 560, 594, 606 and 853 $cm^{-1}$ could be related to cristobalite (C), whitlockite (W) and hydromagnezite (HM) in accordance with our preliminary results [32]. Furthermore, the bands posited at 654, 853, 960, 1009, 1024 and 1111 $cm^{-1}$ can be assigned to the presence of HA in the C1F composite [41]. In the FTIR spectrum of the C2F composite obtained (Fig. 3, curve b) we can observe some absorption bands at 520, 543, 606, and 840 $cm^{-1}$, which are indicative for crystalline HA structures. In addition, the peaks at 868, 939 and 1060 $cm^{-1}$ can be assigned to the silicocarnotite (S) formed in the studied composite [41,42]. The absorption maxima, visible at ~720 $cm^{-1}$ could be related to the presence of HM and amide V. From the FTIR presented results, we can conclude that our data are in accordance with our previous XRD results [32].

### *3.2. Samples after in vitro test in 1.5 SBF solution*

XRD results obtained for the composites immersed in 1.5 SBF solutions for 14 days in static conditions are presented in Figs. 4 and 5 (and summarized in Table 1). From the presented data it can be seen that XRD patterns are quite different. In the case of the C1F composite (Fig. 4) the obtained HA (PDF card 01-072-7532) has a high crystallinity. On the other hand, the crystallinity of W and HM was slightly decreased after immersion in 1.5 SBF solutions for 14 days of soaking. In the case of the C2F sample (Fig. 4) the crystallinity of

**Table 1. IR vibration modes and their assignments observed for the C1F and C2F samples, after *in vitro* test in SBF**

| Vibration mode | IR for C1F sample [$cm^{-1}$] | IR for C2F sample [$cm^{-1}$] | Literature |
|---|---|---|---|
| $\nu_2$ $PO_4^{3-}$ | 458 | | [45] |
| $\nu_2$ $PO_4^{3-}$ | 472 | 475 | [46,48] |
| $\nu_4$ $PO_4^{3-}$ | 545 | | [51] |
| $\nu_4$ $PO_4^{3-}$ | | 562 | [46,51,54] |
| $\nu_4$ $PO_4^{3-}$ | 591 | | [51,52] |
| $\nu_4$ $PO_4^{3-}$ | | 686 | [50] |
| calcite | 712 | 712 | [53,64] |
| vaterite | 743 | 744 | [53,67] |
| aragonite | 856 | | [64] |
| $\nu_2$ $CO_3^{2-}$ | | 875 | [45,47,55] |
| $\nu_3$ $CO_3^{2-}$ | 1410 | 1413 | [52,54,55,57,60] |
| $\nu_3$ $PO_4^{3-}$ | 1040 | 1023 | [48,49] |
| $\nu_3$ $PO_4^{3-}$ | 1065 | 1040 | [48,49,68] |
| $\nu_3$ $CO_3^{2-}$ | 1420 | 1424 | [47,54,58,61] |
| $\nu_3$ $CO_3^{2-}$ | 1431 | 1430 | [49] |
| calcite | 1440 | 1440 | [63,64] |
| $\nu_3$ $CO_3^{2-}$ | 1457 | 1452 | [55,56,58,62] |
| $\nu_3$ $CO_3^{2-}$ | 1470 | 1468 | [57] |
| $\nu_3$ $CO_3^{2-}$ | 1480 | 1483 | [65] |
| $\nu_3$ $CO_3^{2-}$ | 1491 | 1492 | [47] |
| $\nu_3$ $CO_3^{2-}$ | 1503 | 1501 | [48,58,59] |
| $\nu_3$ $CO_3^{2-}$ | 1516 | 1517 | [31] |
| $\nu_3$ $CO_3^{2-}$ | 1530 | 1534 | [31] |
| $\nu_3$ $CO_3^{2-}$ | 1552 | 1552 | [52,55] |
| $\nu_3$ $CO_3^{2-}$ | 1570 | 1571 | [48] |

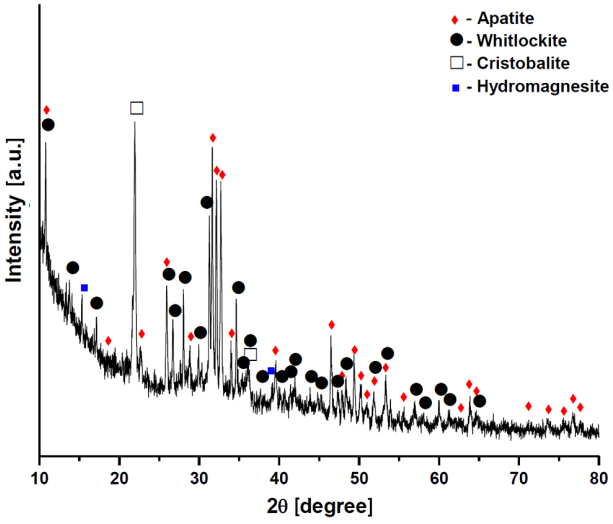


**Figure 4. XRD pattern of C1F sample, after soaking in SBF solution for 14 days**

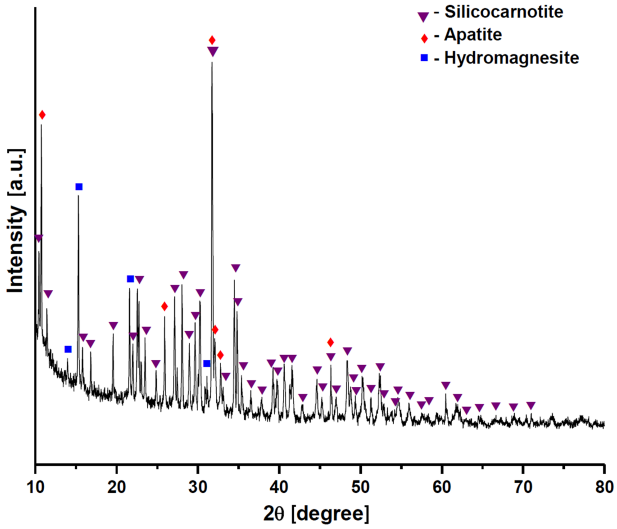


**Figure 5. XRD pattern of C2F sample, after soaking in SBF solution for 14 days**

HA observed on the surface of the immersed sample has the lowest crystallinity. In the same composite, the crystallinity of HM and S phases has been decreased, i.e. they were partially dissolved in 1.5 SBF solutions during the immersion time. As can also be seen, in both synthesized and immersed composites, XRD detects the presence of fibroin amorphous halo. The obtained results are in a good agreement with some of our preliminary results [43].

FTIR data of the C1F and C2F composites, after soaking in SBF solution for 14 days are presented in Fig. 6. From the FTIR data, it can be seen that the presented spectra are similar to those of HA/protein composites previously reported by Yang *et al.* [44]. On the other hand, for two composites obtained after immersion process, the FTIR spectrum (Fig. 6, curve a) exhibits the presence of C at 795 $cm^{-1}$, HM at 591 and 851 $cm^{-1}$ and HA at 545, 960, and 1111 $cm^{-1}$ [32]. Fur-

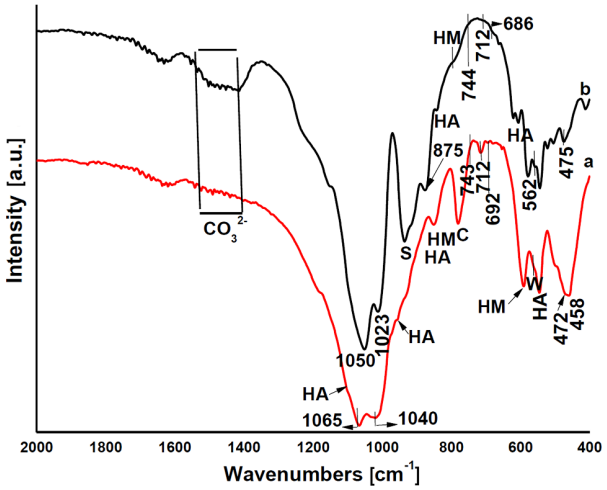


**Figure 6. FTIR spectra of C1F (a) and C2F (b) composites after soaking in SBF for 14 days**

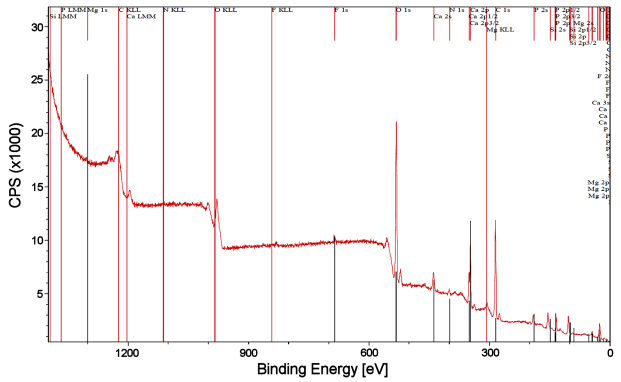


**Figure 7. XPS spectra of survey scan for C1F sample after *in vitro* test in SBF solution for 14 days**

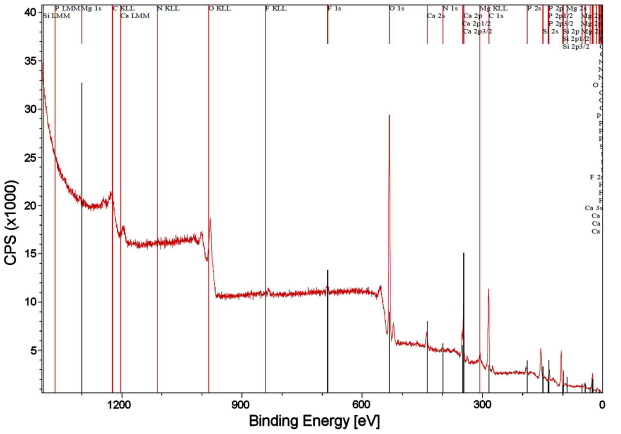


**Figure 8. XPS spectra of survey scan for C2F sample after *in vitro* test in SBF solution for 14 days**

thermore, for the C2F sample (Fig. 5, curve b), the band posited at 939 $cm^{-1}$ can be ascribed to S, and a band at 795 $cm^{-1}$ can be related to the HM, and those at 608 and 840 $cm^{-1}$ are indicative for HA [32]. These data are in a good agreement with XRD results (Figs. 4 and 5). Further, both FTIR spectra also show the presence of $\nu_2$ $PO_4^{3-}$ [45–47], $\nu_3$ $PO_4^{3-}$ [48,49] and $\nu_4$ $PO_4^{3-}$ [46,50–54] modes. For the C2F sample, infrared absorption bands of $\nu_2$ $CO_3^{2-}$ were found at 875 $cm^{-1}$ [45,47,55] and $\nu_3$ $CO_3^{2-}$ from 1410 to 1570 $cm^{-1}$ [31,47–49,52,55–65] correspond to the B-type carbonate substitution ($CO_3^{2-} \longrightarrow PO_4^{3-}$) in HA lattice. It can also be seen that two FTIR spectra display a band posited at ~1500 $cm^{-1}$ which can be attributed to the presence of A-type carbonate substitution ($CO_3^{2-} \longrightarrow OH^-$) in HA lattice [31,48,58,59], as well as to amide II [66]. This finding allows us to confirm the presence of $CO_3^{2-}$ ions within the channels of the HA structure which is in accordance with Ma *et al.* [47]. From the data presented in Table 1 we can conclude that B-type $CO_3$HA (bioapatite) was preferentially formed on the surface of the soaked samples in 1.5 SBF solution [45,47,50,52,54,55,57,58,60,61], accompanied with traces of different $CaCO_3$ phases – vaterite, aragonite and calcite [53,63,64,67].

XPS investigations of the prepared samples, after immersion in 1.5 SBF solutions, were performed to identify chemical states and surface structures obtained. A survey scan XPS spectra for the C1F and C2F samples immersed in 1.5 SBF for 14 days in static conditions are shown in Figs. 7 and 8. The selected scan areas of XPS spectra for both samples immersed for 14 days in 1.5 SBF solutions are given in Fig. 9. The C1s peak position due to the adventitious carbon was detected at the binding energy (BE) value of 285 eV. The peak positions of different chemical states are listed in Table 2.

In the pure HA the peaks at 345.5 and 347.5 eV (Ca2p) and 133.5, 133.7 eV (P2p) and 531.1, 531.3 eV (O1s) confirm the presence of apatite groups [69–72]. In addition, the peaks for Ca2p with BE at 347.7 eV can also be described for Si-HA structures with different quantity of silicon, as has been published by Solla *et al.* [70]. On the other hand, the O1s spectrum indicates the presence of two additional peaks with BE values at 532.6 eV (for both samples) and 533.6 eV (for the C1F sample) and 533.8 eV (for the C2F sample). The first one may correspond to the adsorbed $H_2O$ on

**Table 2. XPS profile parameters for Ca2p, O1s, Si2p, P2p and C1s states for different samples obtained on the surface, after *in vitro* test in 1.5 SBF solutions for 14 days of soaking in static conditions**

| Binding energy (BE) [eV] | | | | | | | | | |
|---|---|---|---|---|---|---|---|---|---|
| Ca2p | | O1s | | Si2p | | P2p | | C1s | |
| C1F | C2F | C1F | C2F | C1F | C2F | C1F | C2F | C1F | C2F |
| 345.5 | 347.5 | 531.3 | 531.1 | 103.3 | 103.5 | 133.5 | 133.7 | 285.0 | 285.0 |
| 347.5 | | 532.6 | 532.6 | | | | | | |
| | | 533.3 | 533.8 | | | | | | |

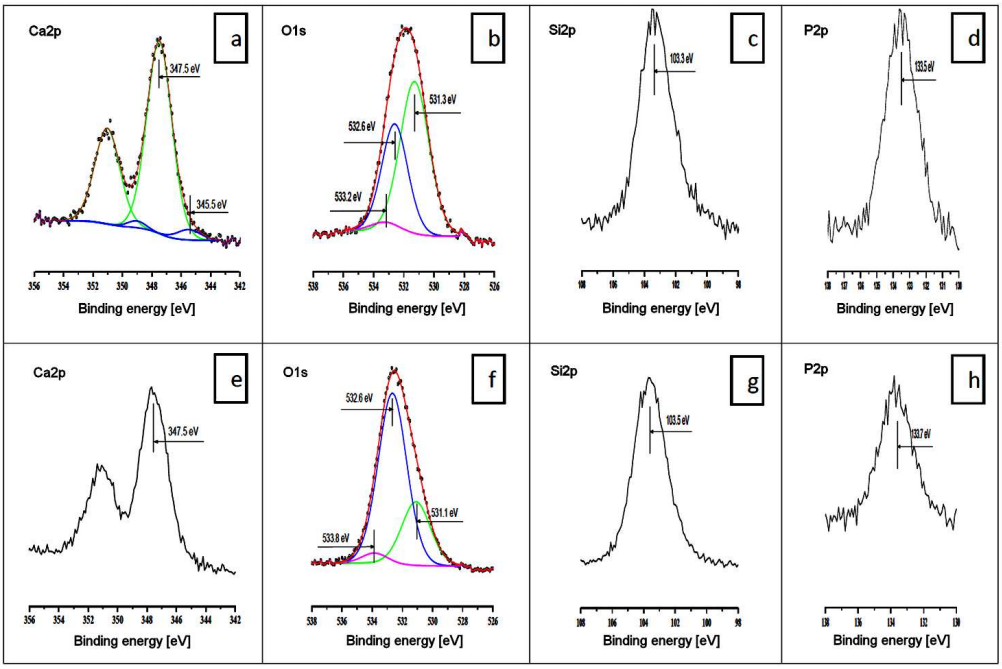


**Figure 9. XPS spectra of selected scan areas for C1F and C2F samples, after soaking in SBF solution for 14 days: Ca2p (a, e), O1s (b, f), Si2p (c, g), and P2p (d, h)**

the deposits [72]. The second one indicate the presence of $H_2O$ ads., in accordance with Taube *et al.* [73]. The Si2p peak at 103.5 eV can be related to Si–O bond of $SiO_2$ probably from cristobalite [74] in accordance with our XRD results (Fig. 2). Finally, the well resolved peak at 285.0 eV (data are not shown here) can be related to the presence of $C_xH_y$ in accordance with Ni and Ratner [75].

It is well known that, it should be possible to distinguish between the various calcium phosphate phases by measuring the atomic fractions of Ca and P from XPS. Thus, the surface compositions of the C1F and C2F composites are presented in Table 3. Chusuei *et al.* found that in practice, the measured Ca/P ratios were all consistently lower than the theoretical Ca/P value [76]. In our case, Ca/P ratio for the C1F sample (1.52 at.%) is closely related to the $CO_3HA$ [76], while the Ca/P ratio for the C2F sample (1.79 at.%) is slightly higher than the expected for the stoichiometric HA (1.66) [77]. The slightly elevated Ca/P ratio observed here in the XPS results may also be a consequence of calcium enrichment of the uppermost surface of the HA derived coatings, as it has been previously observed by other authors [71,76,78]. In summary, the XPS study indicates the formation of HA in our deposits, and corroborates the XRD and FTIR results.

Figure 10 presents the ICP-AES data for the evaluation of the ionic concentrations of Ca, Si, P and Mg in

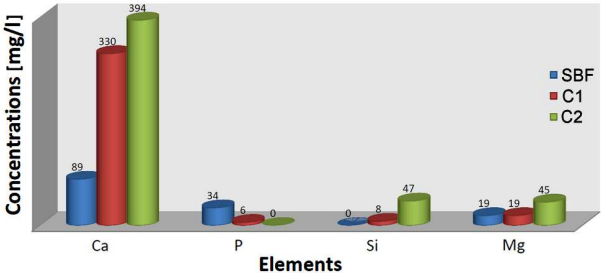


**Figure 10. ICP-AES for C1F and C2F samples after immersion in SBF solution for 14 days**

the 1.5 SBF solutions after soaking of the obtained samples for 14 days in static conditions. The Ca rate for the C1F and C2F composites shows similar behaviour. The quantity of Ca increases to 330 and 394 mg/l compared with the Ca concentration of the initial 1.5 SBF solution (89 mg/l). The observed concentrations are in relation with the weight ratio of the C1 and C2 glass ceramics in the composites (80 wt.%), and the processes of partial dissolution of W, S, HA and HM under the experimental conditions are in agreement with XRD data (Figs. 4 and 5). In accordance with our preliminary results [31,32], the P concentration (6 and 0.5 mg/l) is probably the limiting factor for the growth of the $CO_3HA$ layer on the surface of the synthesized composites. The equal rate of Mg for the C1F sample (19 mg/l) with Mg content in 1.5 SBF solution (19 mg/l) can be explained with the

**Table 3. Concentration of the elements on the surfaces of C1F and C2F samples immersed in SBF for 14 days**

| Elements (chemical state) | C (C1s) | Si (Si2p) | P (P2p) | Cl (Cl2p) | Ca (Ca2p) | N (N1s) | O (O1s) | Mg (Mg1s) | Ca/P [at.%] |
|---|---|---|---|---|---|---|---|---|---|
| C1F | 47.32 | 10.59 | 5.07 | 0.64 | 7.73 | 1.03 | 27.62 | <0.5 | 1.52 |
| C2F | 36.57 | 17.61 | 3.36 | 0.01 | 6.01 | 0.69 | 35.75 | <0.5 | 1.79 |

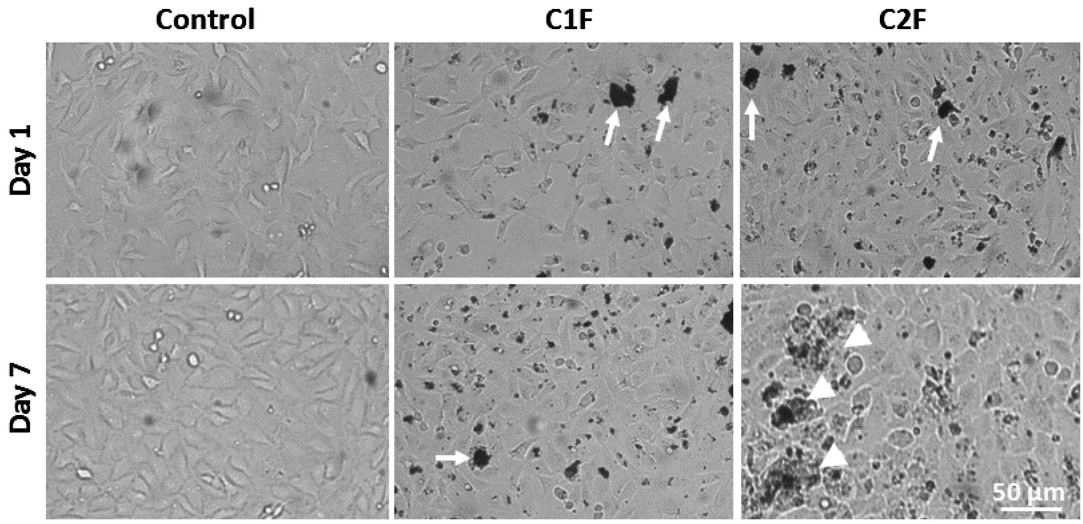


**Figure 11. Phase contrast micrograph, showing MG63 cell proliferation following treatment with 10 µg/cm$^2$ of C1F or C2F at different time points (the arrow showed the formation of bioglasses aggregates and the arrowheads denote the formation of refringent matrix around the granules)**

low crystallinity of HM in the composite in agreement with XRD data depicted in Fig. 1. The highest Mg content for the C2F sample (45 mg/l) can be related to the presence of HM with high crystallinity as can be seen from Fig. 2. Furthermore, the Si content increased from 8 mg/l (for the C1F sample) to 47 mg/l (for the C2F sample). This fact could be related to the phase composition of the samples (Figs. 2 and 4). On the other hand, cristobalite has a low dissolution rate in comparison with S in SBF solution.

Furthermore, both prepared composites were tested in a cytotoxicity assay on MG63 cells. The results showed that there was no effect of toxicity in the concentration range from 1 to 10 µg/cm$^2$ of C1F or C2F from day 1 to day 7. Phase contrast microscopy showed that on the first day following the treatment, the cells were attached and spread on the culture dishes, exhibiting a polygonal morphology (Fig. 10). The aggregate formation at the C1F and C2F samples in cell culture media was also clearly visible (Fig. 11). Possessing a normal rate of cell division, the cells proliferated and reached confluence on the third day, immobilizing the granules in the cell layer. Thereafter, the cells piled up around the granules forming refringent multilayers (Fig. 11). The MG63 cells did not show any evidence of advanced differentiation, during the studied period, and no significant morphological differences were noted between the two substances used for treatment of cultures were noted.

A number of studies have shown that ionic products released from glass-ceramics by dissolution, creating a favourable environment for osteoblast proliferation and differentiation *in vivo*. However, the high bioactivity index could result in a rapid pH shift of the culture medium *in vitro* that may be unfavourable for cellular metabolism. To study this process we additionally examined the effect of the C1F and C2F on the MG63 mineralization in period up to 21 days, as an indicator of advanced cell differentiation. The formation of calcium nodules was detected by ARS staining. As illustrated in Fig. 12, differentiation induced by calcium nodules were observed in MG63 cells treated with both composites for 21 days. Cells were treated with 10 µg/cm$^2$ of C1F (Fig. 12A) or C2F (Fig. 12B). All cells were stained with Alizarin Red S to detect the calcium nodules and analysed at magnification of 40×. The cycles represent an area, where the cells form calcium nodules in contact with composites.

In order to determine the bioactivity of MG63 cells, cultured in the presence of C1F and C2F composites, we focused on their alkaline phosphatase (ALP) activity, as this enzyme is a common indicator of the expression of the osteoblastic phenotype. Figure 13 shows the ALP activity of MG63 cells cultured with C1F and C2F for 7 and 21 days. The ALP activity of the MG63 cells cultured for 7 days with C1F and C2F did not differ significantly. However, the ALP activity of the MG63 cells cultured with the C2F was slightly higher than those for the other samples cultured with the C1F composite. In

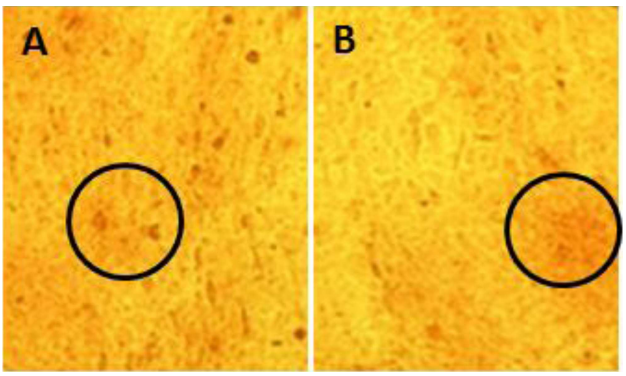


**Figure 12. Insoluble calcium nodules (red) formed in MG63 cells undergoing differentiation for composite: a) C1F and b) C2F**

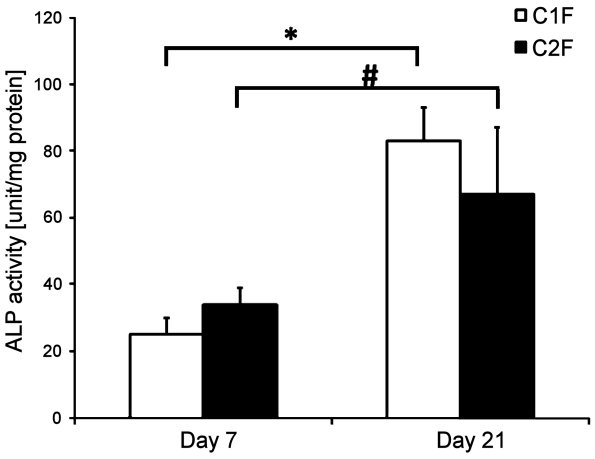


**Figure 13. ALP activity in MG63 monolayer growing in the presence of C1F and C2F, determined from three replicate cultures, shown as the mean ±SD (* $p < 0.010$, # $p < 0.033$)**

particular, the ALP activity of MG63 cells cultured with the C1F and C2F composites was approximately 4-fold higher on day 21 than that on day 7.

## IV. Conclusions

The two novel glass-ceramics in the $CaO$-$SiO_2$-$P_2O_5$-MgO system, after soaking in TRIS-HCl solution, have been used for the synthesis of silk fibroin/glass-ceramic composites in 20 : 80 weight ratio by mixing method. After synthesizing the two samples, XRD proved the presence of different crystalline phases such as hydroxyapatite, whitlockite, cristobalite, silicocarnotite and hydromagnezite. FTIR of the prepared composites showed the presence of basic absorption bands corresponding to the organic and inorganic phases of the composites.

After *in vitro* test in 1.5 SBF solutions for 14 days in static conditions, XRD revealed the presence of HA. On the other hand, the crystallinity of whitlockite, hydromagnezite and silicocarnotite slightly decreased, i.e. these phases partially dissolved in 1.5 SBF solutions during the soaking time. Furthermore, FTIR depicted that B-type $CO_3$HA (bioapatite) was preferentially precipitated on the soaked surfaces. XPS of the immersed samples proved that HA was formed on the composites. ICP-AES measurements lead us to conclude that in C2F sample silicon substituted $CO_3$HA can be formed on the soaked surface. The biological experiments with MG63 osteosarcoma cells led us to resume that the prepared composites create a favourable environment for osteoblast proliferation and differentiation *in vivo*. In this context, the ALP activity of the MG63 cells cultured for 7 days with C1F and C2F did not differ significantly. However, the ALP activity of the MG63 cells cultured with C2F was slightly higher than those for the other samples cultured with C1F. In particular, the ALP activity of MG63 cells cultured with C1F and C2F composites was approximately 4-fold higher on day 21 than that on day 7.

## References

1. S.R. Stock, "The mineral-collagen interface in bone", *Calcif. Tissue Int.*, **97** (2015) 262–280.
2. K. Lin, C. Wu, J. Chang, "Advances in synthesis of calcium phosphate crystals with controlled size and shape", *Acta Biomater.*, **10** [10] (2014) 4071–4102.
3. J. Brzezińska-Miecznik, K. Haberko, M. Sitarz, M.M. Bućko, B. Macherzyńska, "Hydroxyapatite from animals bone - Extraction and properties", *Ceram. Int.*, **41** (2015) 4841–4846.
4. S.L. McNamara, J. Rnjak-Kovacina, D.F. Schmidt, T.J. Lo, D.L. Kaplan, "Silk as a biocohesive sacrificial binder in the fabrication of hydroxyapatite load bearing scaffolds", *Biomaterials*, **35** (2014) 6941–6953.
5. S. Liao, M. Ngiam, F. Watari, S. Ramakrishna, C.K. Chan, "Systematic fabrication of nano-carbonated hydroxyapatite/collagen composites for biomimetic bone grafts", *Bioinspira. Biomimetics*, **2** [3] (2007) 37–42.
6. X. Liu, L.A. Smith, J. Hu, P.X. Ma, "Biomimetic nanofibrous gelatin/apatite composite scaffolds for bone tissue engineering", *Biomaterials*, **30** [12] (2009) 2252–2258.
7. M. Lee, W. Li, R.K. Siu, J. Whang, X. Zhang, C. Soo, K. Thing, B.M. Wu, "Biomimetic apatite-coated alginate/chitosan microparticles as osteogenic protein carriers", *Biomaterials*, **30** [30] (2009) 6094–6101.
8. X. Cai, H. Tong, X. Shen, W. Chen, J. Yan, J. Hua, "Preparation and characterization of homogeneous chitosan-polylactic acid/hydroxyapatite nanocomposite for bone tissue engineering and evaluation of its mechanical properties", *Acta Biomater.*, **5** [7] (2009) 2693–2703.
9. X. Zhang, Y. Li, G. Lv, Y. Zuo, Y. Mu, "Thermal and crystallization studies of nano-hydroxyapatite reinforced polyamide 66 biocomposites", *Polym. Degrad. Stabil.*, **91** [5] (2006) 1202–1207.
10. T. Furuzono, A. Kishida, J. Tanaka, "Nano-scaled hydroxyapatite/polymer composite I. Coating of sintered hydroxyapatite particles on poly(gammamethacryloxy propyltrimethoxysilane) grafted silk fibroin fibers through chemical bonding", *J. Mater. Sci.*, **15** (2004) 19–23.
11. X.D. Kong, F.Z. Cui, X.M. Wang, M. Zhang, W. Zhang, "Silk fibroin regulated mineralization of hydroxyapatite nanocrystals", *J. Cryst. Growth*, **270** [1-2] (2004) 197–202.
12. H.H. Kim, J.B. Park, M.J. Kang, Y. Park, "Surface-modified silk hydrogel containing hydroxyapatite nanoparticle with hyaluronic acid-dopamine conjugate", *Int. J. Biol. Macromol.*, **70** (2014) 516–522.
13. M. Ribeiro, M.A. de Moraes, M.M. Beppu, M.P. Garcia, M.H. Fernandes, F.J. Monteiro, M.P. Ferraz, "Development of silk fibroin/nanohydroxyapatite composite hydrogels for bone tissue engineering", *Eur. Polym. J.*, **67** (2015) 66–77.
14. X. He, X. Huang, Q. Lu, Sh. Bai, H. Zhu, "Nanoscale control of silks for regular hydroxyapatite formation", *Prog. Nat. Sci.: Mater. Int.*, **22** [2] (2012) 115–119.
15. L.-P. Yan, J. Silva-Correia, M.B. Oliveira, C. Vilela, H. Pereira, R.A. Sousa, J.F. Mano, A.L. Oliveira, J.Mo. Oliveira, R.L. Reis, "Bilayered silk/silk-nano CaP scaffolds for osteochondral tissue engineering: In vitro and in vivo assessment of biological performance", *Acta Biomater.*, **12** (2015) 227–241.
16. A. Teimouri, M. Azadi, R. Emadi, J. Lari, A.N. Chermahini, "Preparation, characterization, degradation and

biocompatibility of different silk fibroin based composite scaffolds prepared by freeze-drying method for tissue engineering application", *Polym. Degrad. Stabil.*, **121** (2015) 18–29.
17. R. Nemoto, S. Nakamura, T. Isobe, M. Senna, "Direct synthesis of hydroxyapatite-silk fibroin nano-composite sol via a mechanochemical route", *J. Sol-Gel Sci. Technol.*, **21** [1-2] (2001) 7–12.
18. L. Wang, R. Nemoto, M. Senna, "Effects of alkali pretreatment of silk fibroin on microstructure and properties of hydroxyapatite-silk fibroin nanocomposite", *J. Mater. Sci: Mater. Med.*, **15** [3] (2004) 261–265.
19. Ch. Du, J. Jin, Y. Lia, X. Kong, K. Weic, J. Yao, "Novel silk fibroin/hydroxyapatite composite films: Structure and properties", *Mater. Sci. Eng. C*, **29** [1] (2009) 62–68.
20. R. Nemoto, L. Wang, T. Ikoma, J. Tanaka, M. Senna, "Preferential alignment of hydroxyapatite crystallites in nanocomposites with chemically disintegrated silk fibroin", *J. Nanopart. Res.*, **6** [2] (2004) 259–265.
21. Y. Ren, X. Sun, F. Ciu, "Effects of pH and initial $Ca^{2+}$–$H_2PO_4^-$ concentration on fibroin mineralization", *Front. Mater. Sci.*, **1** [3] (2007) 258–262.
22. L.-P. Yan, J. Li, G. Xu, H. He, X. Ye, Y. Chen, X. Cheng, J. Fu, D. He, "Facile fabrication of nano-hydroxyapatite/silk fibroin composite via a simplified coprecipitation route", *J. Mater. Sci.*, **45** [21] (2010) 5814–5819.
23. L. Wang, Ch. Li, M. Senna, "High-affinity integration of hydroxyapatite nanoparticles with chemically modified silk fibroin", *J. Nanopart. Res.*, **9** [5] (2007) 919–929.
24. T. Furuzono, K. Ishihara, N. Nakabayashi, Y. Tamada, "Chemical modification of silk fibroin with 2-methacryloyloxyethyl phosphorylcholine. II. Graft-polymerization onto fabric through 2-methacryloyloxyethyl isocyanate and interaction between fabric and platelets", *Biomaterials*, **21** [4] (2000) 327–333.
25. R. Kino, T. Ikoma, A. Monkawa, S. Yunoki, M. Munekata, J. Tanaka, T. Asacura, "Deposition of bone-like apatite on modified silk fibroin films from simulated body fluid", *J. Appl. Polym. Sci.*, **99** [5] (2006) 2822–2828.
26. Y. Li, Y. Cai, X. Kong, J. Yao, "Anisotropic growth of hydroxyapatite on the silk fibroin films", *Appl. Surf. Sci.*, **255** [5] (2008)11681–11685.
27. X. Kong, X. Sun, F. Cui, Ch. Ma, "Effect of solute concentration on fibroin regulated biomineralization of calcium phosphate", *Mater. Sci. Eng. C*, **28** [4] (2006) 639–643.
28. L. Li, K-M. Wei, F. Lin, X-D. Kong, J-M. Yao, "Effect of silicon on the formation of silk fibroin/calcium phosphate composite", *J. Mater. Sci.*, **19** [2] (2008) 577–582.
29. H. Zhu, J. Shen, X. Feng, H. Zhang, Y. Guo, J. Chen, "Fabrication and characterization of bioactive silk fibroin/wollastonite composite scaffolds", *Mater. Sci. Eng. C*, **30** [1] (2010) 132–140.
30. N. Vachiraroj, J. Ratanavaraporn, S. Damrongsakkul, R. Pichyangkura, T. Banaprasert, S. Kanokpanont, "A comparison of Thai silk fibroin-based and chitosan-based materials on in vitro biocompatibility for bone substitutes", *Int. J. Biol. Macromol.*, **45** (2009) 470–477.
31. L. Radev, T. Gerganov, H. Georgiev, A. Kolev, V. Vassileva, R. Yankova, E. Cholakova, "Silk fibroin/calcium phosphate silicate composites: In vitro bioactivity", *Int. J. Mater. Chem.*, **3** [3A] (2013) 8–15.
32. L. Radev, I. Michailova, H. Georgiev, D. Zaimova, "Carbonate apatite formation on novel multiphase CaO-$SiO_2$-$P_2O_5$-MgO glass-ceramics in TRIS-HCl buffer", *Process. Appl. Ceram.*, **10** [2] (2016) 57–67.
33. D.A. Shirley, "High-resolution X-ray photoemission spectrum of the valence bands of gold", *Phys. Rev. B*, **5** [12] (1972) 4709–4714.
34. J.H. Scofield, "Hartree-Slater subshell photoionization cross-sections at 1254 and 1487 eV", *J. Electron Spectrosc. Related Phenomena*, **8** [2] (1976) 129–137.
35. T. Mosmann, "Rapid colorimetric assay for cellular growth and survival: Application to proliferation and cytotoxicity assays", *J. Immunol. Methods*, **65** [1-2] (1983) 55–63.
36. C.A. Gregory, W.G. Gunn, A. Peister, D.J. Prockop, "An Alizarin red-based assay of mineralization by adherent cells in culture: comparison with cetylpyridinium chloride extraction", *Anal. Biochem.*, **329** (2004) 77–84.
37. H.W. Kaufman, I. Kleinberg, "Studies on the incongruent solubility of hydroxyapatite", *Calcif. Tissue Int.*, **27** [2] (1979) 143–151.
38. L. Brazda, D. Rohanova, A. Helebrant, "Kinetics of dissolution of calcium phosphate (Ca-P) bioceramics", *Process. Appl. Ceram.*, **2** [1] (2008) 57–62.
39. H. Cao, X. Chen, L. Huang, Zh. Shao, "Electrospinning of reconstituted silk fiber from aqueous silk fibroin solution", *Mater. Sci. Eng. C*, **29** (2009) 2270–2274.
40. S. Shang, L. Zhu, J. Fan, "Physical properties of silk fibroin/cellulose blend films regenerated from the hydrophilic ionic liquid", *Carbohyd. Polym.*, **86** (2011) 462–468.
41. S. Serena, M.A. Sainz, A. Caballero, "Single-phase silicocarnotite synthesis in the subsystem $Ca_3(PO_4)_2$-$Ca_2SiO_4$", *Ceram. Int.*, **40** [6] (2014) 8245–8252.
42. S. Serena, A. Caballero, P.N. de Aza, M.A. Sainz, "New evaluation of the in vitro response of silicocarnotite monophasic material", *Ceram. Int.*, **41** [8] (2015) 9411–9419.
43. L. Radev, M.H.V. Fernades, I.M. Salvado, D. Kovacheva, "Organic/inorganic bioactive materials. Part III: in vitro bioactivity of gelatin/silicocarnotite hybrids", *Cent. Eur. J. Chem.*, **7** [4] (2009) 721–730.
44. X.J. Yang, C.Y. Liang, Y.L. Cai, K. Hu, Q. Wei, Z.D. Cui, "Recombinant human-like collagen modulated the growth of nano-hydroxyapatite on NiTi alloy", *Mater. Sci. Eng. C*, **29** [1] (2009) 25–28.
45. I. Rehman, W. Bonfield, "Characterization of hydroxyapatite and carbonated apatite by photo acoustic FTIR spectroscopy", *J. Mater. Sci.*, **8** [1] (1997) 1–4.
46. N. Vandecandelaere, Ch. Rey, Ch. Drouet, "Biomimetic apatite-based biomaterials: on the critical impact of synthesis and post-synthesis parameters", *J. Mater. Sci: Mater. Med.*, **23** [11] (2012) 2593–2606.
47. J. Ma, C.Z. Chen, D.G. Wang, X.G. Meng, J.Z. Shi, "In vitro degradability and bioactivity of mesoporous CaO-MgO-$P_2O_5$-$SiO_2$ glasses synthesized by sol-gel method", *J. Sol-Gel Sci. Technol.*, **54** [1] (2010) 69–76.
48. I.R. Gibson, W. Bonfield, "Novel synthesis and characterization of an AB-type carbonate-substituted hydroxyapatite", *J. Biomed. Mater. Res. A*, **59** [4] (2002) 697–708.
49. J. Barralet, S. Best, W. Bonfield, "Carbonate substitution in precipitated hydroxyapatite: An investigation into the effects of reaction temperature and bicarbonate ion concentration", *J. Biomed. Mater. Res. A*, **41** [1] (1998) 79–86.
50. G. Penel, G. Leroy, C. Rey, E. Bres, "MicroRaman spectral

study of the $PO_4$ and $CO_3$ vibrational modes in synthetic and biological apatites", *Calcif. Tissue Int.*, **63** [6] (1998) 475–481.
51. Ch. Rey, M. Shimizu, B. Collins, M.J. Glimcher, "Resolution-enhanced Fourier transform infrared spectroscopy study of the environment of phosphate ions in the early deposits of a solid phase of calcium-phosphate in bone and enamel, and their evolution with age. I: Investigations in the $\nu_4$ $PO_4$ domain", *Calcif. Tissue Int.*, **46** [6] (1990) 384–394.
52. D.P. Minh, N.D. Tran, A. Nzihou, P. Sharrock, "Carbonate-containing apatite (CAP) synthesis under moderate conditions starting from calcium carbonate and orthophosphoric acid", *J. Mater. Sci. Eng. C*, **33** [5] (2013) 2971–2980.
53. H. El Feki, Ch. Rey, M. Vignoles, "Carbonate ions in apatites: Infrared investigations in the $\nu_4$ $CO_3$ domain", *Calcif. Tissue Int.*, **49** [4] (1991) 269–274.
54. T. Takeshita, Y. Matsuura, S. Arakawa, M. Okamoto, "Biomineralization of hydroxyapatite on DNA molecules in SBF: morphological features and computer simulation", *Langmuir*, **29** [38] (2013) 11975–11981.
55. R.Z. LeGeros, O.R. Trautz, E. Klein, J.P. LeGeros, "Two types of carbonate substitution in the apatite structure", *Experientia*, **25** [1] (1968) 5–7.
56. J.P. Lafon, E. Champion, D. Bernache-Assollant, R. Gibert, A.M. Danna, "Termal decomposition of carbonated calcium phosphate apatites", *J. Thermal. Anal. Calorim.*, **72** [3] (2003) 1127–1134.
57. M.E. Fleet, "Infrared spectra of carbonate apatites: $\nu_2$-Region bands", *Biomaterials*, **30** [8] (2009) 1473–1481.
58. M. Vignoles, G. Bonel, D.W. Holcomb, R.A. Young, "Influence of preparation conditions on the composition of type B carbonated hydroxyapatite and on the localization of the carbonate ions", *Calcif. Tissue Int.*, **43** [1] (1988) 33–40.
59. C. Rey, V. Renugopalakrishnan, M. Shimizu, B. Collins, M.J. Glimcher, "A resolution-enhanced Fourier Transform Infrared spectroscopic study of the environment of the $CO_3^{2-}$ ion in the mineral phase of enamel during its formation and maturation", *Calcif. Tissue Int.*, **49** [4] (1991) 259–268.
60. J.E. Barralet, G.J.P. Fleming, C. Campion, J.J. Harris, A.J. Wright, "Formation of translucent hydroxyapatite ceramics by sintering in carbon dioxide atmospheres", *J. Mater. Sci.*, **38** [19] (2003) 3979–3993.
61. Y. Yusufoglu, M. Akinc, "Effect of pH on the carbonate incorporation into the hydroxyapatite prepared by an oxidative decomposition of calcium-EDTA chelate", *J. Am. Ceram. Soc.*, **91** [1] (2008) 77–82.
62. F. Apfelbaum, H. Diab, I. Mayer, "An FTIR study of carbonate in synthetic apatites", *J. Inorg. Biochem.*, **45** [7] (1992) 277–282.
63. Ch. Zaman, A. Takeuchi, Q.H.M. Zaman, K. Ischikawa, "Fabrication of B-type carbonate apatite blocks by the phosphorization of free-molding gypsum-calcite composite", *Dental Mater. J.*, **27** [5] (2008) 710–715.
64. S. Gopi, V.K. Subramanian, K. Palanisamy, "Aragonite–calcite–vaterite: A temperature influenced sequential polymorphic transformation of $CaCO_3$ in the presence of DTPA", *Mater. Res. Bull.*, **48** [5] (2013) 1906–1912.
65. D.N. da Rocha, L. de Andrade Gobbo, M.H. Prado da Silva, "Production and characterization of niobate apatite", *J. Mater. Res. Technol.*, **2** [1] (2013) 24–29.
66. M. Chang, W. Douglas, J. Tanaka, "Organic-inorganic interaction and the growth mechanism of hydroxyapatite crystals in gelatin matrices between 37 and 80 °C", *J. Mater. Sci.*, **17** [4] (2006) 387–396.
67. B. Yang, Zh. Nan, "Abnormal polymorph conversion of calcium carbonate from calcite to vaterite", *Mater. Res. Bull.*, **47** [3] (2012) 521526.
68. I. Michailova, L. Radev, V. Aleksandrova, I. Colova, I.M.M. Salvado, M.H.V. Fernandes, "Carbonata-apatite forming ability of polyphase glass-ceramics in the CaO-MgO-$SiO_2$ system", *IUCTM*, **50** [4] (2015) 502–511.
69. S. Kaciulis, G. Monttogno, L. Pandolfi, M. Cavalli, G. Giappi, "XPS study of apatite-based coatings prepared by sol-gel methoid", *Appl. Surf. Sci.*, **151** [1-2] (1999) 1–5.
70. E.L. Solla, J.P. Borrajo, P. Gonzalez, J. Serra, S. Chiussi, "Pulsed laser deposition of silicon-substituted hydroxyapatite coatings", *Vacuum*, **82** (2008) 1383–1385.
71. A.R. Boyd, L. Rutledge, L.D. Randolph, B.J. Meenan, "Stroncium-substituted hydroxyapatite coatings deposited via co-deposition sputter technique", *J. Mater. Sci. Eng. C*, **46** (2015) 290–300.
72. R.-J. Chung, M.-F. Hsieh, R.N. Panda, T-S. Chin, "Hydroxyapatite layers deposited from aqueous solutions on hydrophilic silicon substrate", *Surf. Coatings Technol.*, **165** (2013) 194–200.
73. F. Taube, R. Ylmen, A. Shchukarev, S. Nietzsche, J.G. Noren, "Morphologycal and chemical characterization of tooth enamel exposed to alkaline agents", *J. Dentistry*, **38** (2010) 72–81.
74. B.Y. Park, S. Lee, K. Park, Ch.H. Bae, S.M. Park, "Enhancement of light emission from silicon nanocrystals by post-$O_2$-annealing process", *J. Appl. Phys.*, **107** (2010) 014314.
75. M. Ni, B.D. Ratner, "Differentiation of calcium carbonate polymorphs by surface analysis techniques – An XPS and TOF-SIMS study", *Surf. Interface Anal.*, **40** [10] (2008) 1356–1361.
76. Ch.C. Chusuei, D.W. Goodman, M.J. Van Stipdonk, D.R. Justes, E.A. Schweikert, "Calcium phosphate phase identification using XPS and time-of-flight cluster SIMS", *Anal. Chem.*, **71** (1998) 149–153.
77. H.-Y. Shin, J.-Y. Jung, S.-W. Kim, W.-K. Lee, "XPS analysis on chemical properties of calcium phosphate thin films and osteoblastic HOS cell responses", *J. Ind. Eng. Chem.*, **12** [3] (2006) 476–483.
78. A.R. Boyd, C. O'Kane, B.J. Meenan, "Control of calcium phosphate thin film stoichiometry using multi-target sputter deposition", *Surf. Coat. Technol.*, **233** (2013) 131–139.